Phytomedicine Plus 5 (2025) 100684

Contents lists available at ScienceDirect

Phytomedicine Plus

journal homepage: www.sciencedirect.com/journal/phytomedicine-plus

Ficus deltoidea standardized methanolic extract improves kidney structure and function against streptozotocin-induced diabetic nephropathy in rats

Nurdiana Samsulrizal [a,*], Noor Syaffinaz Noor Mohamad Zin [a], Nur Syimal`ain Azmi [a], Mohd Daud Bakar [b], Hafandi Ahmad [c], Yong-Meng Goh [c]

[a] TuAH Industrial Research, Lab with Bio Fluid Sdn Bhd, Faculty of Applied Sciences, Universiti Teknologi MARA, 40450 Shah Alam, Selangor, Malaysia
[b] Bio Fluid Sdn Bhd, 70, Jalan Bulan U5/172, Subang 2, 40150 Shah Alam, Selangor, Malaysia
[c] Department of Veterinary Preclinical Sciences, Faculty of Veterinary Medicine, Universiti Putra Malaysia (UPM), 43400 Serdang, Selangor, Malaysia

ARTICLE INFO

Keywords:
Chemometrics
Ficus deltoidea
FTIR
Kidney
Streptozotocin-induced diabetes

ABSTRACT

Background: Oxidative stress and peripheral insulin resistance are the key pathogenesis of diabetic nephropathy. We have previously demonstrated that *Ficus deltoidea* increases insulin secretion and improves tissue regeneration by reducing oxidative stress in diabetic rats. However, it remains uncertain whether *F. deltoidea* could delay the progression of nephropathy.

Hypothesis/Purpose: This study aimed to examine the nephroprotective effects of *F. deltoidea* on streptozotocin-induced diabetic nephropathy in rats.

Methods: High-Performance Liquid Chromatography (HPLC) was used to identify the flavonoid compounds in the leaf extract of *F. deltoidea*. The methanolic extract of *F. deltoidea* was administered orally at 1000 mg/kg body weight for eight weeks to diabetic rats. Serum creatinine, urea, uric acid, total bilirubin, and urinary creatinine were measured to estimate kidney function. Enzyme-linked immunosorbent assays (ELISA) assessed the levels of oxidative stress, antioxidants, and apoptosis-related proteins in the kidney tissue. The spectral markers related to nephroprotective activity were predicted using Fourier-transform infrared (FTIR) spectroscopy combined with chemometric analysis. Histomorphometric evaluations were performed on the kidney sections stained with hematoxylin and eosin (H&E).

Results: HPLC identified the presence of vitexin, isovitexin, quercetin, and kaempferol in *F. deltoidea* methanolic leaves extract. The biochemical and histological examinations consistently showed that *F. deltoidea* extract improved kidney structure and function by reducing oxidative stress and apoptosis. We noticed that biochemical and pathological changes corresponded to the infrared (IR) peaks at 1545 cm^{-1} and 1511 cm^{-1} (amide II), 1246 cm^{-1} (DNA/RNA phosphate backbones), and 1181 cm^{-1} (C–O vibrations). Multivariate analysis of IR spectra demonstrated that the diabetic rats treated with *F. deltoidea* extract had a similar clustering pattern to that of the normal animals.

Conclusion: These findings indicate that the methanolic extract of *F. deltoidea* exhibits nephroprotective activity. FTIR spectroscopy may be useful for monitoring structural and biochemical alterations in the kidney during diabetes treatment.

Abbreviations

Bcl-2	B-cell lymphoma-2
Casp 8	Caspase-8
Casp 9	Caspase-9
DC	Diabetic control group
DFD	*F. deltoidea*-treated diabetic group
DMET	Metformin-treated diabetic group
DN	Diabetic nephropathy
ELISA	Enzyme-linked immunosorbent assays
FTIR	Fourier Transform Infrared
GBM	Glomerular basement membrane
GFR	Glomerular filtration rate
GPX	Glutathione peroxidase

* Corresponding author.
E-mail address: nurdiana7251@uitm.edu.my (N. Samsulrizal).

https://doi.org/10.1016/j.phyplu.2024.100684

Available online 16 November 2024

HPLC	High-Performance Liquid Chromatography
IR	Infrared
JNK	c-Jun NH2-terminal kinase
MDA	Malondialdehyde
NC	Normal control group
p53	Tumor protein
ROS	Reactive oxygen species
SOD	Superoxide dismutase
STZ	Streptozotocin
Tris-HCl	Tris hydrochloride

Introduction

Diabetic nephropathy (DN) is a significant complication of long-standing hyperglycemia. It is characterized by proteinuria, glomerulosclerosis, the glomerular basement membrane (GBM) thickening, and tubulointerstitial fibrosis (Pillai et al., 2023). Animal and human studies consistently support DN as the leading cause of end-stage kidney failure and account for 30-40 % of patients entering kidney transplant programs (Banki et al., 2014). It has been reported that DN increased mortality risk by 25 % (González-Pérez et al., 2021). These data indicate that there are aspects of diagnosis and pathogenesis that are not fully understood and are responsible for hyperglycemia and diabetes, persisting to be the major cause of kidney disease.

Poor glycemic control and the accumulation of reactive oxygen species (ROS) play a significant role in the development of DN (Hirata et al., 2015). The glomerulus is particularly vulnerable to ROS attack attributed to the presence of heparan sulfate proteoglycans, the anionic polysaccharides of the GBM (Singh et al., 2013; Borza et al., 2017). However, recent studies have shown that all kidney cells, such as mesangial cells, podocytes, and tubulointerstitial cells, are also liable to be affected by hyperglycemia (Guo et al., 2020). Sustained kidney biochemical alterations have been observed in these kidney cells even after tight glycemic control (de Oliveira et al., 2017). The diagnosis of DN conventionally involves assessing renal function through urine tests, blood tests, imaging studies, and monitoring of blood pressure and kidney function markers. However, these diagnostic methods have been reported to have lower specificity and sensitivity in early detection. Drozdz et al. (2020) and Mata-Miranda et al. (2017) suggest a positive correlation between the structural and biochemical changes of the kidney tissue and the infrared (IR) absorption spectra. Their findings imply that FTIR could present a promising avenue to enhance the diagnostic process for DN.

FTIR spectroscopy is a simple, label-free, and highly reproducible analytical technique. The application of FTIR spectroscopy combined with chemometrics identifies the specific molecular fingerprint of biological samples, which in turn provides clues to the biochemical and pathological changes. FTIR spectroscopy supported with quantitative and qualitative spectra analysis has been shown possible to discriminate between benign and cancer tissue (Sablinskas et al., 2020; Yu et al., 2017). Several earlier studies have also demonstrated the advantages of FTIR spectroscopy as a non-invasive technique for elucidating the chemical features of cells and tissues (Ashtarinezhad et al., 2015; Movasaghi et al., 2008; Holman et al., 2003), in part attributed to chronic complications of diabetes. The success in the application of FTIR spectroscopy for the detection of glucose in serum (Bernardes-Oliveira et al., 2020; Petibois et al., 1999), whole blood (Shen et al., 2003), and urine samples (Pezzaniti et al., 2001) has previously been reported. FTIR spectroscopy has been successfully used for monitoring apoptotic cell death (Mihoubi et al., 2017) and antioxidant activity (Barraza-Garza et al., 2016). Our previous studies demonstrated that FTIR spectroscopy could be used to provide a systemic snapshot and relevant to monitor the pancreas and brain pathological changes of diabetic rats (Nurdiana et al., 2017a, 2017b). However, analysis of the structure and biochemical changes of diabetic kidney disease by FTIR remains uninvestigated, and this is where the novelty of the current research lies.

F. deltoidea (Moraceae) is an evergreen shrub or small tree that is easily found in Malaysia and widely distributed in Southeast Asian countries such as Thailand, Sumatra, Java, Kalimantan, Sulawesi, and the Moluccas. The decoction of *F. deltoidea* has traditionally been used in postpartum care specifically to improve uterine strength, regain energy, and prevent postpartum bleeding (Sulaiman et al., 2008; Salleh et al., 2013). It is also served as a health tonic or taken as herbal tea to relieve headaches, fever, and toothache (Bunawan et al., 2014). Acute toxicity studies showed that the median lethal dose (LD_{50}) of aqueous and ethanolic leaf extracts of *F. deltoidea* was greater than 5000 mg/kg b.wt (Farsi et al., 2013) and 2000 mg/kg b.wt (Nugroho et al., 2020), respectively. Moreover, investigations have also shown that *F. deltoidea* leaf extracts do not exert cytotoxic effects on normal liver (Abrahim et al., 2018) and kidney (Apriasari et al., 2024) cells, implying their biocompatibility. Our previous work has demonstrated that treatment with *F. deltoidea* leaf extract decreased blood glucose, increased insulin secretion, and enhanced pancreatic islet regeneration in STZ-induced diabetic rats (Nurdiana et al., 2017a). We also found *F. deltoidea* extract possesses neuroprotective properties, improving spatial learning and memory and cortical gyrification patterns (Nurdiana et al., 2017b). Although the synergy between antioxidant, antidiabetic, tissue regenerative, and neuroprotective effects on kidney function has extensively been reported (Jiménez-Osorio et al., 2016; Anvarifard et al., 2023; Barbieri et al., 2024), the potential of *F. deltoidea* against DN remains largely unexplored. This gap in knowledge highlights the importance of investigating the nephroprotective effects of *F. deltoidea* to expand our understanding of its comprehensive therapeutic capabilities. Therefore, our study was primarily designed to assess kidney function by measuring biochemical and histological changes in response to the treatment of *F. deltoidea* extract. We also test the hypothesis that FTIR spectroscopy, in combination with multivariate analyzes, would be able to identify the spectral markers corresponding to the biochemical and pathological changes in the kidneys of diabetic rats.

Materials and methods

Plant material and extract preparation

The leaves of *F. deltoidea* var. *kunstleri* were purchased from Moro Seri Utama Enterprise, Batu Pahat, Johor, Malaysia. The plant material was identified and authenticated by a specialized taxonomist. A voucher specimen (UKMB-40315) was deposited in the Herbarium Unit, Universiti Kebangsaan Malaysia for further reference. The leaves were washed thoroughly, oven-dried at 37 ± 5 °C, ground to a fine powder in an electric grinder, and weighed. The powdered leaves (100 g) were soaked in 1 L absolute methanol for three days at room temperature as described by Ashraf *et al.* (2020). Liquid extracts were concentrated using a rotary vacuum evaporator (R-215, Buchi, Switzerland) under reduced pressure. The extraction yield of *F. deltoidea* was 10.6 %. The extracts were kept in tightly closed glass containers and stored at -20 °C until further use.

HPLC analysis

Chromatographic conditions: Methanolic extract of *F. deltoidea* leaves were separated and identified using HPLC equipped with an ultraviolet-visible detector (Agilent 1100 series; Agilent Technologies, Santa Clara, CA, USA). Chromatographic separation was performed using a Luna C18 column (250 × 4.6 mm, 5 µm, Phenomenex, USA) at 40 °C. A mobile phase consists of a mixture of solvent A (ammonium acetate, pH 5.0) and solvent B (acetonitrile: methanol; 90:10). The mobile phase gradient is as follows: 85 % solvent A and 15 % solvent B (t = 0 min), 75 % solvent A and 25 % solvent B (t = 20 min), 55 % solvent A and 45 % solvent B (t = 30 min), 5 % solvent A and 95 % solvent B (t = 35-37 min), and 85 % solvent A and 15 % solvent B (t = 40-45 min). The flow rate was 1.5 mL/min. The injection volume was 10 µL and the

signal was monitored at 270 nm.

Standard and sample preparation: A standard mixture stock solution (30 µg/mL) was prepared in methanol/dimethylsulfoxide (3:1, v/v) by weighing out approximately 0.0060 g of the analyte into a 20 mL volumetric flask. The methanolic extract of *F. deltoidea* at a concentration of 24 mg/mL was prepared in ethanol. All samples were stored in the dark at a low temperature (5 °C) and filtered through a 0.20 µm nylon syringe filter before HPLC analysis.

Peak characterization: The compounds were identified by comparing retention times and absorbance spectrum profiles.

Animals

A total of 42 male Sprague-Dawley rats weighing around 100-200 g were purchased from Chennur Suppliers, Malaysia. The condition of animals was assessed upon arrival following the institutional standard operating procedure for health monitoring of rodents. We observed each animal daily to assess its health and well-being during the experiment. A visual examination of the rats upon arrival is valuable in determining any need for immediate treatment. Several criteria have been used to evaluate the health status of rats including behavior modification (prostration, agitation, lethargy, and aggressiveness), skin lesions (hair loss, rarefied hair, areata alopecia, and easy hair removal), respiratory abnormalities (cough, sneeze, wheeze, hemoptysis), diarrhea and weight variation. None of these signs were seen in animals within 2 weeks of arrival. The animals were housed in polypropylene cages (47 × 34 × 20 cm) and maintained under standard laboratory conditions with a 12 h light/dark cycle, at a temperature of 25 ± 1 °C, throughout the study. Animals were fed with standard rat chow (Gold Coin Holdings, Kuala Lumpur, Malaysia) and tap water *ad libitum* before and during the experiments. Animals were euthanized by terminal exsanguination under anesthesia with ketamine (80 mg/kg) and xylazine (8 mg/kg) 8 weeks after treatment (Nurdiana et al., 2017b). All study protocols, including DN induction and sacrifice operation, were performed in strict accordance with the guidelines of the National Research Council for the Care and Use of Laboratory Animals. The study was approved by the ethics review board of Universiti Putra Malaysia, Animal Care and Use Committee (UPM/IACUC/AUP-R090/2019).

Animal models of DN

Taking into consideration that the success rate of diabetic induction by STZ was 50-60 % (Wang et al., 2014) and the total survival rate of animals aged between 6–11 weeks was 97 % (Wang-Fischer and Garyantes, 2018), a total of 36 male rats received a single intraperitoneal injection of 0.5 mL STZ (Sigma-Aldrich, Deisenhofen, Germany) at a dosage of 60 mg/kg of body weight (Nurdiana et al., 2017a). STZ has been reported to induce DN in rats and is a reliable animal model that displays progressive tubular damage and glomerular injury, presenting histological features that resemble human DN (Alaofi, 2020). However, most of the studies on DN are largely restricted to male rats, as female rats have been reported to be less sensitive to STZ (Deeds et al., 2011; Noshahr et al., 2020) and exhibit fluctuating sex hormone levels (Shepard, 2019). Seven days after STZ treatment, the fasting blood glucose levels were determined using a blood glucose meter (Accu-Chek Performa, Roche, Germany). Animals with fasting blood glucose levels above 11 mmol/L (n = 18) for three consecutive days were selected for further analyzes, while those outside this range (n = 15) were excluded from the study (Dong et al., 2014). Animals that are not expected to survive until the next scheduled evaluation after STZ injection (n = 3) were humanely euthanized by using cervical dislocation.

Experimental design

Eighteen diabetic rats after STZ treatment were randomly divided into three groups of six rats each. The treatment schedule was as follows:

Group diabetic control (DC): The diabetic rats were treated with 0.5 mL saline (n = 6).

Group metformin-treated diabetic rats (DMET): The diabetic rats were treated with 1000 mg/kg body weight of metformin (n = 6).

Group *F. deltoidea*-treated diabetic rats (DFD): The diabetic rats were treated with 1000 mg/kg body weight of *F.deltoidea* (n = 6).

Six age-matched normal rats were used as normal control (NC): The normal rats were administered with 0.5 mL saline.

Metformin was selected as a positive control as it has been shown to attenuate renal inflammation, oxidative stress, glomerular sclerosis, and tubular fibrosis in type 1 diabetes rats (Jain et al., 2020). Dose selection for *F. deltoidea* and metformin is according to research reported by Farsi *et al.* (2014) and Tahara *et al.* (2008), respectively. The dose is considered safe as the LD_{50} of metformin in rodents was reported greater than 1500 mg/kg/day (Takemori et al., 2020) while *F. deltoidea* is higher than 5000 mg/kg/day (Farsi et al., 2013). All treatments were given once daily via oral gavage for eight weeks.

Experimental procedure

At the end of the experiment, all animals were fasted overnight to reduce variability in basal blood glucose (Jensen et al., 2013). The terminal urine was collected for 4 h immediately preceding sacrifice in individual metabolic cages. Blood samples (10-15 mL) were collected via cardiac puncture from the rats, centrifuged at 4000 *g* for 15 min, and serum was stored in aliquots at -80 °C. Both kidneys were harvested and weighed. The kidney weight index was calculated as the percentage of kidney weight to the body weight. Half of the kidney was kept in 10 % formalin for tissue characterization, and the other half was stored at -80 °C before biochemical analysis. Serum creatinine, urea, uric acid, and total bilirubin were determined by the auto analyzer (Hitachi 911, Boehringer-Mannheim, Germany).

Glomerular filtration rate

Glomerular filtration rate (GFR) based on creatinine clearance was determined using urine and serum creatinine assay kits (Cayman, MI, USA) as well as urine output levels. GFR was calculated using the following formula:

$$\mathrm{FR}\left(\frac{\mathrm{mL}}{\mathrm{min}}\right) = \frac{\text{Urinary creatinine } \left(\frac{\mathrm{mg}}{\mathrm{mL}}\right) \text{ X Urine volume (mL) X } 1000}{\text{Serum creatinine } \left(\frac{\mathrm{mg}}{\mathrm{mL}}\right) \text{ X time (min)}}$$

Determination of spot urine creatinine

The spot urine creatinine was determined quantitatively using enzyme-linked immunosorbent assays (Cayman, MI, USA). ELISA tests were conducted in triplicate and performed according to the manufacturer's protocol.

Preparation of Tissue Homogenates

One hundred milligrams of kidney tissue was homogenized in a homogenizing buffer (50 mM Tris-HCl, 1.15 % KCl pH 7.4) using a Teflon pestle (Glass-Col, USA) at 900 rpm. The homogenates were centrifuged at 9,000 *g* in a refrigerated centrifuge (4 °C) for 10 min to remove nuclei and debris. The supernatant obtained was used for FTIR analysis and biochemical assays. Protein concentration was estimated by the method of Lowry *et al.* (1951), using bovine serum albumin as the standard.

FTIR analysis

FTIR measurements were performed to analyze the structural and

biochemical properties of the kidney of the rats. The FTIR spectra were recorded using a Bruker 66V FTIR spectrometer (Bruker Corp., MA, USA). Twenty microliters of kidney homogenate were deposited on a liquid cell (demounted cell) using a pipette according to the method reported by Demir *et al.* (2015). All spectra were recorded over the range 4000-400 cm^{-1} frequency range versus a clean prism background at room temperature. Three spectra were recorded for each treatment group. Spectra analysis was performed using OPUS 7.0 software (Bruker Optics, GmbH).

All the spectra were pre-processed, and the second derivative spectra were calculated using the Savitzky-Golay algorithm. Second derivative spectra were taken using a 20-point smoothing factor to resolve differences in peak intensities among experimental animals. Second derivative spectra were further used to quantify the features of interest by integration and statistical assessment using Origin Pro 2021. The fingerprint region from 1800-800 cm^{-1} was used for all subsequent data analyzes. IR spectra were predicted based on the peak intensities obtained from the integrated peak area of the selected frequency limits.

Chemometric analyzes

All the registered spectra were subjected to multivariate analysis (MVA), including hierarchical cluster analysis (HCA) and principal component analysis (PCA). All analyzes were conducted using the OriginPro 2021 software (OriginLab, Northampton, MA, USA). The unsupervised analysis of PCA and HCA was performed for a general overview of clustering patterns.

Estimations of apoptosis-related protein levels

The levels of Casp 8, JNK, Casp 9, p53, and Bcl-2 in the kidney supernatant were measured by a double-antibody sandwich ELISA, using a commercially available kit from Qayee-Bio (Shanghai, China) according to the manufacturer's instructions. The absorbance was determined spectrophotometrically at a wavelength of 450 nm using a spectrophotometer (Epoch 2 microplate spectrophotometer, BioTek Instruments, Inc, Vermont, USA).

Biochemical estimations in kidney homogenates

Kidney oxidative stress biomarkers such as glutathione peroxidase (GPX), superoxide dismutase (SOD), and malondialdehyde (MDA) levels were determined using commercially available assay kits (Cayman, MI, USA). The absorbance change vs time for each biomarker was measured spectrophotometrically at a specific wavelength using a spectrophotometer (Epoch 2 microplate spectrophotometer, BioTek Instruments, Inc, Vermont, USA).

Histomorphometric evaluation

The kidney was fixed in 4 % formaldehyde in phosphate-buffered saline (Invitrogen, Carlsbad, CA), embedded in paraffin blocks, sectioned at 4 μm, and stained with hematoxylin and eosin (H&E). All slides were examined using light microscopy (Motic BA410, Wetzlar, Germany) equipped with a digital camera (Moticam Pro 285A, Wetzlar, Germany). The degree of glomerular sclerosis and tubular atrophy scores were determined on H&E stained paraffin sections adopting the method proposed by Sari *et al.* (2020). The semiquantitative histopathological scoring scheme is presented in Table 1. The glomerulosclerosis scores were obtained after observation under light microscopy at 400X total magnification. The glomerular score of each animal was expressed as a mean value of 100 glomeruli. The tubular injury was assessed at a total magnification of 100X. A total of 10 microscopic fields from each animal were selected for a semiquantitative scoring system of tubular lesions.

Table 1
Glomerular sclerosis and tubular atrophy grading system.

Histopathological features	Definition
Glomerulosclerosis	
0	normal glomeruli
1	sclerosis area <25 % (minimal)
2	sclerosis area 25–50 % (moderate)
3	sclerosis area 50–75 % (moderate to severe)
4	sclerosis area >75 %-100 % (severe)
Tubular injury	
0	normal tubules
1	tubular injury <25 %,
2	tubular injury between 25 – 50 %,
3	tubular injury between 50 – 75 %
4	tubular injury >75 %.

Statistical analysis

Results were presented as the mean ±SD and dissected using the Statistical Package for the Social Sciences (SPSS) 26 software (IBM Corporation, USA). The differences between the groups were tested using one-way ANOVA followed by Duncan's multiple-range test. All analysis was performed at a 95 % confidence level.

Results

HPLC analysis of F. deltoidea leaf extract

Compounds vitexin, isovitexin, quercetin, and kaempferol were found to elute at 10.88, 11.29, 25.62, and 29.36 min, respectively. Chromatograms of the standards and sample solution are shown in Fig. 1

Spectral markers corresponding to structural and biochemical changes in the kidneys of DN rats

Fig 2 (a) shows the kidney FTIR absorption of the experimental groups in the regions of 4000-400 cm^{-1}. The biological fingerprint region (1800-800 cm^{-1}) was selected for further analysis as it provides unique features for discrimination between different biological samples (Mata-Miranda et al., 2019). It has been reported that the region between 2800-1800 cm^{-1} contains no important spectral information whilst the region > 3000 cm^{-1} is sensitive to water content within the tissues (Song et al., 2019). Fig 2 (b) represents the second derivative of the kidney FTIR spectra for the selected spectral regions presented in Fig 2 (a). Six potential peaks of interest (1545 cm^{-1}, 1511 cm^{-1}, 1400 cm^{-1}, 1246 cm^{-1}, 1181 cm^{-1} and 1143 cm^{-1}) were identified by comparing the average second derivative spectra of each group. The most important peaks for describing the variations between the experimental animal groups are marked in Fig 2 (c). An absorption band at 1545 cm^{-1} and 1511 cm^{-1} are related to amide II functional groups of proteins (Lubczak, 2008). The intense band at 1400 cm^{-1} arises from the methyl and methylene groups from lipids and proteins (Balan et al., 2019) whereas the band at 1246 cm^{-1} corresponds to the absorption of DNA/RNA phosphate backbones (Samouillan et al.,2017). Other bands at 1181 cm^{-1} and 1143 cm^{-1}, respectively, are related to C–O vibrations from glycogen and other carbohydrates (Elsacker et al., 2019).

We proceeded to compare the peak intensities obtained from the integrated peak area of the selected frequency limits. Table 2 shows the peak intensity of the six IR features. The intensity of the IR spectra was only significantly different at 1545 cm^{-1}, 1511 cm^{-1}, 1246 cm^{-1}, 1181 cm^{-1} and 1143 cm^{-1}. The intensity of amide II peaks (1545 cm^{-1}, 1511 cm^{-1}) was increased in the DC animals, indicating an increase of β-peptides (Kristoffersen et al., 2019). However, the intensity of peaks decreased significantly following treatment with metformin and *F. deltoidea* extract. The intensity of peak at 1246 cm^{-1}, which corresponds to the PO_2^- and C-O absorption of DNA/RNA polysaccharide backbones, also decreased in the kidney of DMET, and DFD rats as

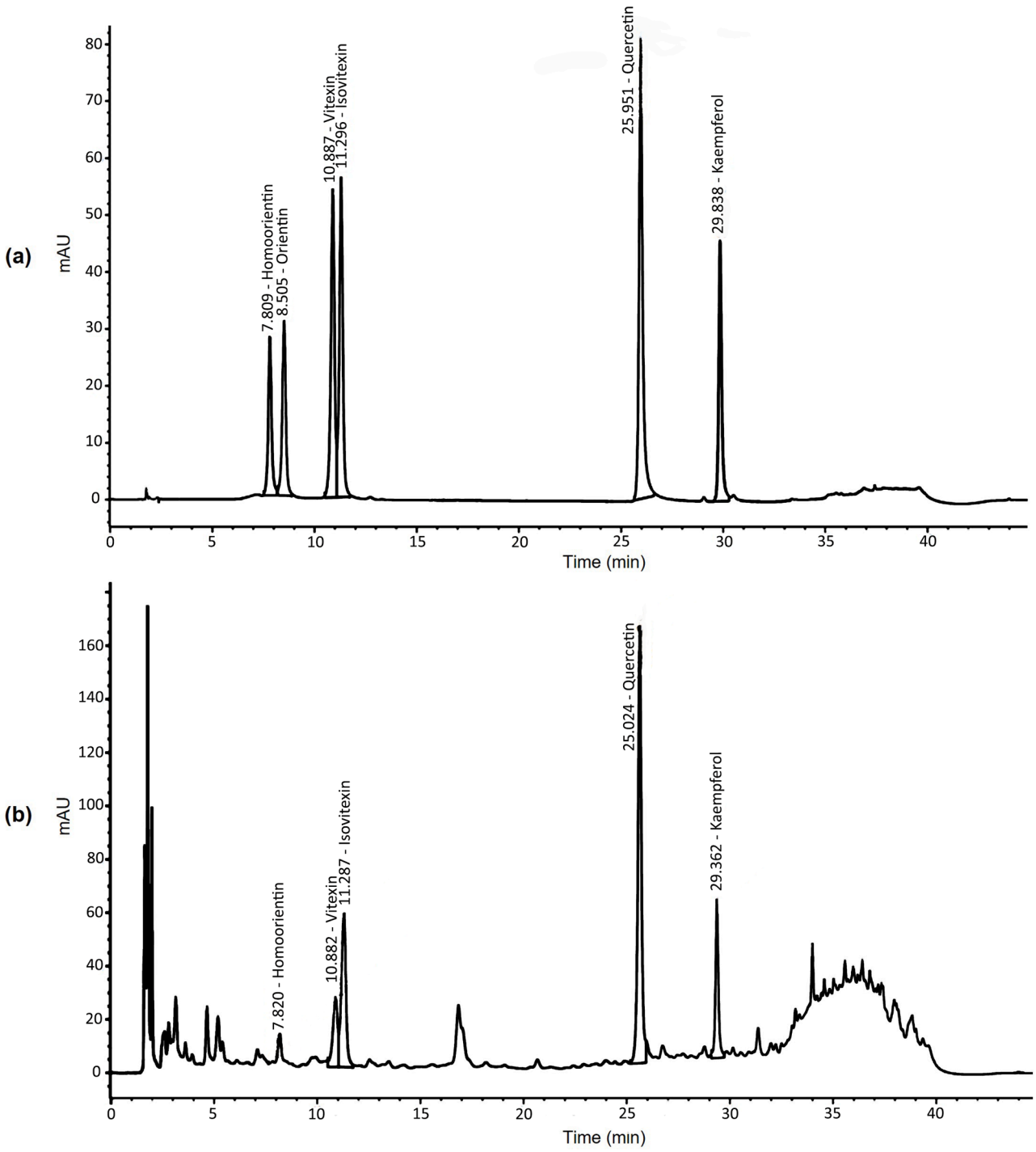

Fig. 1. HPLC-UV-Vis chromatogram of (a) standard mixture of homoorientin, orientin, vitexin, isovitexin, quercetin, and kaempferol (30 ng/mL) (b) methanolic extract of *F. deltoidea* leaves. A mobile phase consisting of a mixture of solvents A (ammonium acetate) and B (acetonitrile containing 0.1 % methanol) and employing a gradient elution (from 85:15 to 5:95, v/v) at a flow rate of 1.5 mL/min. The detection wavelength was set at 270 nm.

compared to the DC group. We observed that the peak intensity of the DFD animals was similar to that of the NC group at 1181 cm^{-1}, whereas the DMET animals had an identical peak intensity at 1143 cm^{-1} to that of the NC group. These results suggest that the peak intensity of FTIR spectra could be relevant to estimating treatment effects from observational data.

Two-way hierarchical clustering heat-map analysis (HCA) was subsequently used to discriminate the extracted dataset filtered by ANOVA ($p < 0.05$) into subgroups according to their similarities. As illustrated in Fig 3 (a), the row tree represents the IR features, the column tree corresponds to the treatment groups, and the colors in the heat table represent the intensities of the IR features dataset. HCA stratified the experimental animals into two major clusters that differed by the relative degree of IR intensities. Cluster I was influenced by the NC, DMET, and DFD groups, while Cluster II seemed to be more related to the DC group.

PCA was performed to verify the empirical clusters produced by HCA. Fig 3 (b) shows the PCA biplot obtained for the first two principal components after PCA with the second derivative spectra of IR features. The first principal component (PC1) explains 62.07 % of the variation

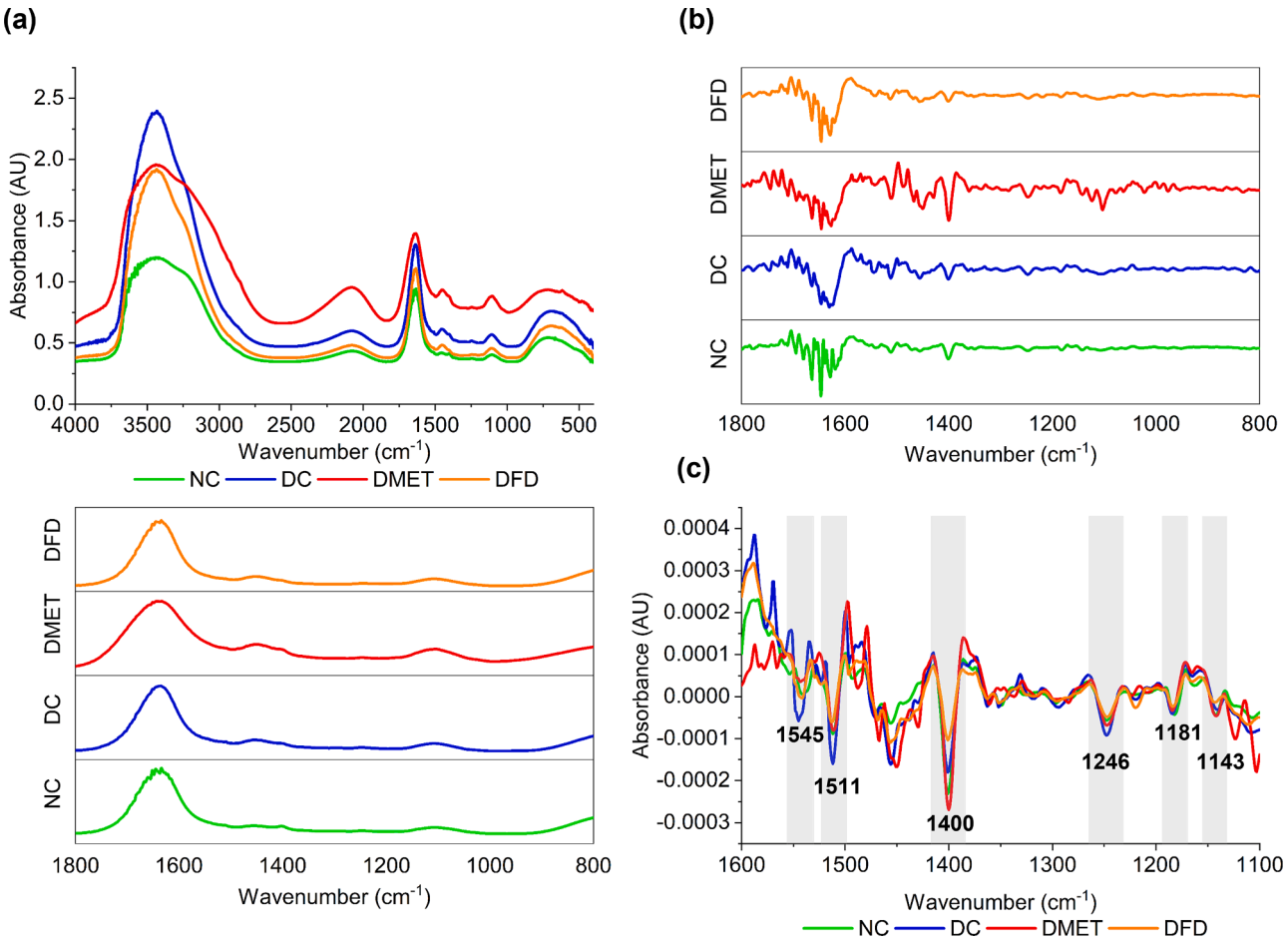

Fig. 2. FTIR analysis of the rat kidney. (a) The average FTIR absorption spectra of kidney tissue in the regions of 4000-400 cm^{-1} (upper graph) and 1800-800 cm^{-1} (lower graph). (b) The average second derivative spectra in the range of 1800-800 cm^{-1} were acquired from the kidneys of the treatment groups. (c) Peaks of interest are potentially relevant to structural and biochemical changes in the rat kidney. The analysis of these spectra was performed on n = 6 animals for each group.

Table 2
The intensity of potential IR marker bands in the kidney of experimental groups.

Peak parameters (cm^{-1})	Frequency limits for integration (cm^{-1})	Groups			
		NC	DC	DMET	DFD
1545	1548 - 1539	0.76 ±	1.42 ±	0.72 ±	0.46 ±
	(IPA x 10^{-3})	0.50^{b}	0.53^{a}	0.54^{b}	0.28^{b}
1511	1514 - 1504	0.18 ±	0.56 ±	0.21 ±	0.27 ±
	(IPA x 10^{-3})	0.03^{b}	0.01^{a}	0.12^{b}	0.11^{b}
1400	1412 - 1392	3.34 ±	2.88 ±	4.02 ±	1.78 ±
	(IPA x 10^{-3})	0.55	1.18	2.45	0.52
1246	1262 - 1239	0.72 ±	1.21 ±	0.79 ±	0.59 ±
	(IPA x 10^{-3})	0.13^{b}	0.30^{a}	0.17^{b}	0.16^{b}
1181	1186 - 1175	0.15 ±	0.24 ±	0.23 ±	0.14 ±
	(IPA x 10^{-3})	0.02^{b}	0.06^{a}	0.01^{a}	0.03^{b}
1143	1148 – 1138	0.61 ±	0.46 ±	0.61 ±	0.22 ±
	(IPA x 10^{-3})	0.12^{a}	0.20^{a}	0.07^{a}	0.11^{b}

All data were subjected to normality Ryan-Joiner (similar to Shapiro-Wilk) and Kolmogorov-Smirnov testing. The data were expressed as mean ± SD (n = 6 in each group) and analyzed by one-way ANOVA followed by the Duncan post hoc test. Superscripts ^{a,b} represents significant differences of IPA among the experimental groups in each of the respective frequencies.

between the five spectroscopic changes, and the second principal component (PC2) accounts for a further 24.15 % of the variation. Together, those two axes explain 86.22 % of the total variance. The PCA analysis also showed that the DC group was separated from the NC and DFD groups by PC1 while the DC and DMET groups were separated by PC2. The loading plot showed that PC1 correlates with the 1545 cm^{-1}, 1511 cm^{-1}, and 1246 cm^{-1}, 1181 cm^{-1}, and 1143 cm^{-1} whereas the spectral features at 1143 cm^{-1} and 1181 cm^{-1} positively contributed to the PC2. We notice that the DC group was completely distinguished from other treatment groups by 1545 cm^{-1}, 1511 cm^{-1}, and 1246 cm^{-1}. The 3D scatter plot of these selected peaks allows comprehensive visualization and separation of the experimental groups [Fig 3 (c)]. The similarity of HCA and PCA results emphasizes the underlying distributions within this dataset. Our data thus suggest that the wavenumbers identified in the fingerprint region can discriminate the nephroprotective effect of treatments with high accuracy.

F. deltoidea extract improves biochemical parameters of DN rats

After 56 days of the experiment, animals in the DC group exhibited significant increases in serum creatinine levels as compared to the NC group. The diabetic rats also showed a significant decrease in urinary creatinine, total serum bilirubin, and glomerular filtration rate (Table 3). Treatment with metformin significantly reduced the serum creatinine by 28.65 % as compared to the DC group. Meanwhile, the level of glomerular filtration rate increased in the DFD group. The serum creatinine and total bilirubin also returned to near-normal levels in response to *F. deltoidea* extract treatment.

F. deltoidea extract decreases apoptosis-protein levels in the kidneys of DN rats

The levels of caspase 8 and caspase 9 were significantly increased in

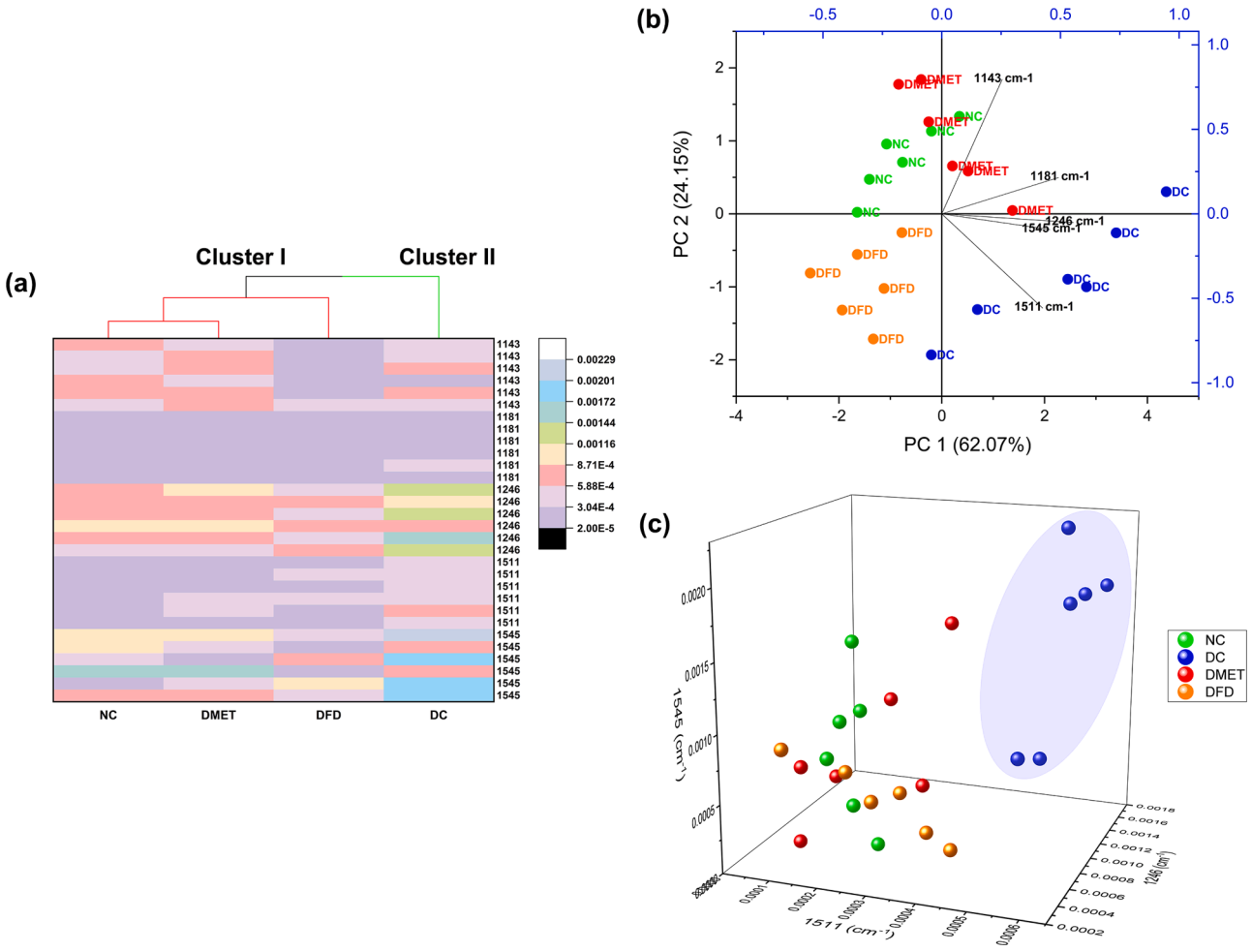

Fig. 3. Chemometric analyzes. (a) Heat-map visualization and cluster tree representation of kidney IR intensities. Each column shows the peak intensities of individual animals from the experimental groups. The amount of each peak intensity is expressed as the total integrated area and is represented by the color scheme. A white and black indicate high and low concentrations of peak intensity, respectively. (b) PCA analysis represents the scores of samples (dots) and loading of variables (vectors) of second derivative spectra of kidney tissue on the first two principal components (86.22 % of total variance). (c) 3D scatter plot of selected peaks displaying the separation of NC, DC, DMET, and DFD groups (n = 6 in each group).

Table 3
Effect of *F. deltoidea* extract on kidney function markers and glomerular filtration rate of the experimental groups.

Parameter	NC	DC	DM	DFD
Serum creatinine (μmol/L)	64.50 ± 2.12[a]	92.50 ± 3.54[b]	66.00 ± 1.41[a]	69.50 ± 2.12[a]
Urinary creatinine (mg/dL)	94.09 ± 3.27[c]	6.81 ± 0.18[a]	9.77 ± 0.36[a]	39.59 ± 9.82[b]
Serum Urea (mmol/L)	9.37 ± 0.97	12.83 ± 1.00	15.80 ± 4.31	10.37 ± 1.70
Serum Uric acid (μmol/L)	213.65 ± 7.43	241.90 ± 49.22	266.30 ± 5.94	183.80 ± 30.55
Total bilirubin (μmol/L)	2.00 ± 0.13[b]	1.00 ± 0.28[a]	1.15 ± 0.21[a]	2.40 ± 0.14[b]
Glomerular filtration rate (mL/min)	2.62 ± 0.19[b]	1.34 ± 0.28[a]	1.60 ± 0.36[a]	4.32 ± 0.52[c]

Values are mean ± SD for six rats in each group. Superscripts [a,b,c] represent significant differences at $p < 0.05$ among the groups within rows

the kidneys of DC rats compared to the NC group (Table 4). However, the DMET and DFD animals had a significant decrease in kidney caspase 8 levels.

Table 4
Apoptosis-related proteins in the kidney tissues of the experimental groups.

Groups	Casp 8 (pg/mg protein)	JNK (pg/mg protein)	Bcl2 (ng/mg protein)	Casp 9 (pg/mg protein)	p53 (ng/mg protein)
NC	376.30 ± 91.15[a]	1300.40 ± 152.13	526.88 ± 11.25[ab]	1007.97 ± 184.89[a]	73.20 ± 20.98
DC	614.44 ± 19.28[c]	1107.54 ± 231.45	541.88 ± 9.44[b]	1368.98 ± 223.68[b]	64.98 ± 11.07
DMET	515.19 ± 24.25[b]	1190.87 ± 108.60	507.71 ± 54.78[a]	1299.54 ± 44.13[b]	57.85 ± 5.49
DFD	496.67 ± 13.65[b]	1069.44 ± 56.66	561.04 ± 17.25[ab]	1260.65 ± 51.62[ab]	66.21 ± 7.68

Data are presented as mean ± SD for six rats in each group. Values with different superscripts in a row differed significantly at $p < 0.05$.

F. deltoidea extract decreases malondialdehyde and improves antioxidants in the kidneys of DN rats

Table 5 shows that the levels of MDA and SOD were significantly increased, whereas GPx activity was significantly decreased in the kidney of the DC group. We have found that SOD and GPx activities increased significantly in the DMET group. In contrast, treatment with *F. deltoidea* extracts resulted in a significant increase in renal GPx and

Table 5
Kidney oxidative stress marker and antioxidant enzymes of various experimental groups.

Groups	Oxidative stress marker	Antioxidant enzymes	
	TBARS (nmol MDA/mg protein)	GPx (U/mg protein)	SOD (mU/mg protein)
NC	4.40 ± 0.036^{a}	242.09 ± 0.950^{c}	4.24 ± 0.551^{a}
DC	19.96 ± 1.179^{c}	83.11 ± 0.309^{a}	6.11 ± 0.706^{b}
DMET	17.26 ± 2.810^{c}	137.38 ± 17.542^{b}	12.79 ± 0.288^{c}
DFD	10.31 ± 0.0453^{b}	207.21 ± 16.491^{c}	7.17 ± 0.698^{b}

Data are presented as mean ± SD for six rats in each group. Values with different superscripts in a row differed significantly at $p < 0.05$.

SOD activities, as well as a significant reduction in MDA values.

F. deltoidea extract alleviates structural changes in the kidneys of DN rats

A histological examination of kidney sections was conducted to confirm the nephroprotective effects. Light microscopic examination revealed normal cytoarchitecture of the kidney in the NC rats [Fig 4 (a)]. However, the kidney structure of DC rats showed marked morphological irregularities. Capillary loops are poorly defined consistent with wider capsular spaces as well as shrinkage hypercellular congested glomeruli. Severe tubular degeneration and tubular necrosis were also noted [Fig 4 (b)]. Histomorphometry analysis showed that the degree of total glomerulosclerosis and tubular injury scores were significantly increased in the DC group by 85.67 % and 93.40 %, respectively as compared to normal rats (Fig 5). Animals in the DC group also had the highest kidney weight index. It was observed that the DMET animals had equally severe changes in the proximal convoluted tubules, which consisted of cytoplasmic vacuolation of tubular epithelial cells and cellular swelling [Fig 4 (c)]. Although some irregular capillaries, in part attached to Bowman's capsule, were noted among the DFD group [Fig 4 (d)], the degree of necrosis of the tubular epithelium was nevertheless lessened by *F. deltoidea* extract. The tubular injury score and kidney weight index were significantly decreased by 77.20 % and 37.11 % in the DFD group. However, there was no difference in the glomerulosclerosis score seen in the DMET and DFD groups.

Discussion

FTIR spectroscopy was applied for the first time to identify spectral markers associated with the nephroprotective effects of *F. deltoidea* extract in diabetic rats. We demonstrated that biochemical and structural changes in the kidneys of rats would leave a signature in the FTIR spectra. Significant differences in the peak intensity at 1545 cm^{-1}, 1511 cm^{-1}, and 1246 cm^{-1} were consistent with observations of increased

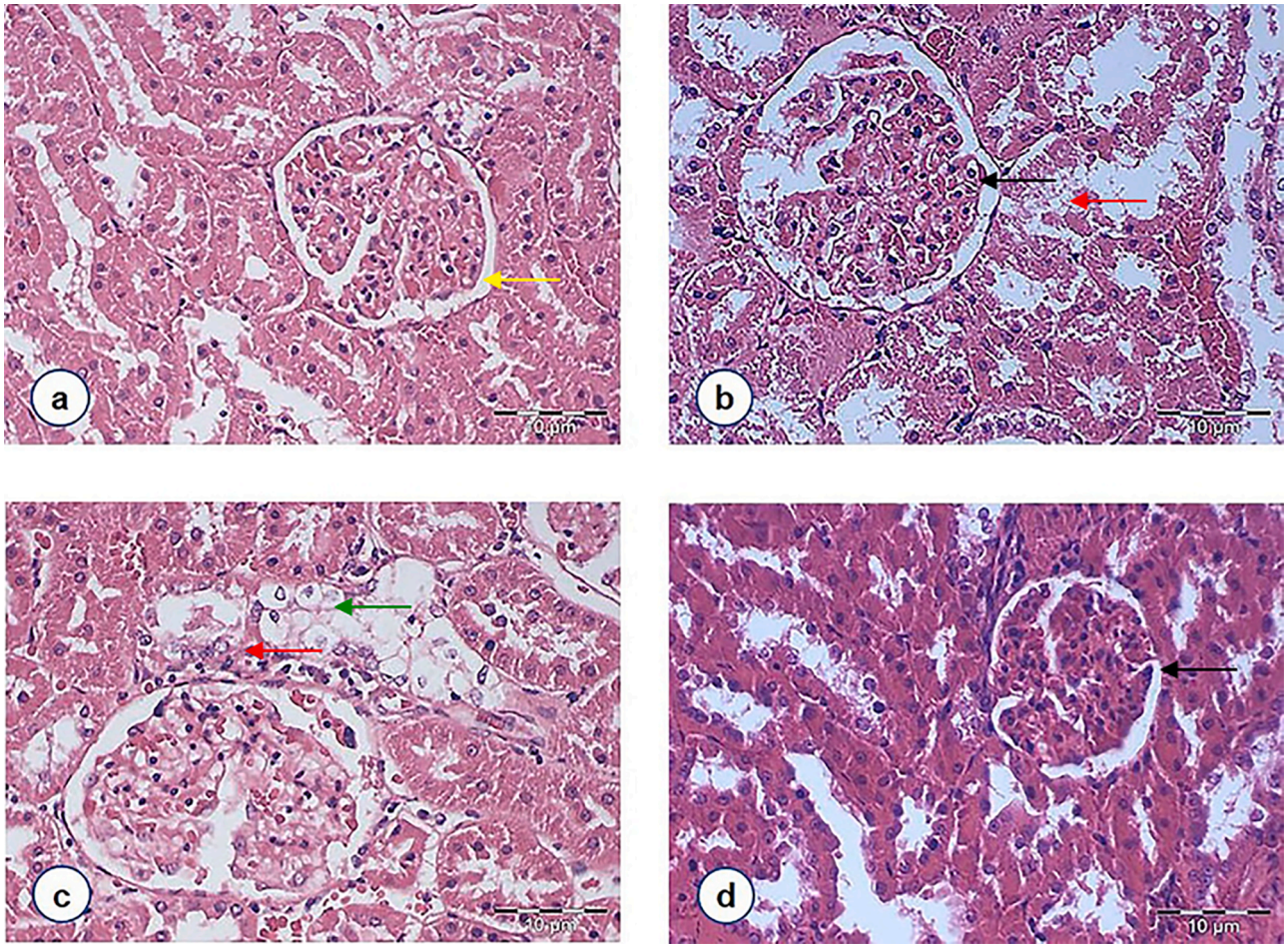

Fig. 4. Light photomicrographs of glomeruli and renal tubules in the kidney of rats from different experimental groups (magnification 400X, HE staining). (a) Normal control rats showing normal glomerulus with parietal cells line the external surface of Bowman space [indicated by the yellow arrow]. (b) STZ-induced diabetic rats depicted a glomerulus with irregular capillaries [indicated by the black arrow] and tubular necrosis [indicated by the red arrow]. (c) Diabetic rats treated with metformin show that the lumina of the tubules is closed by swollen epithelial cells [indicated by the green arrow]. (d) Diabetic rats treated with *F. deltoidea* revealed that the degree of necrosis of the tubular epithelium was lessened by *F. deltoidea* extract, but capillary loops remain poorly defined [indicated by the black arrow]. Images are representative of six animals per experimental group.

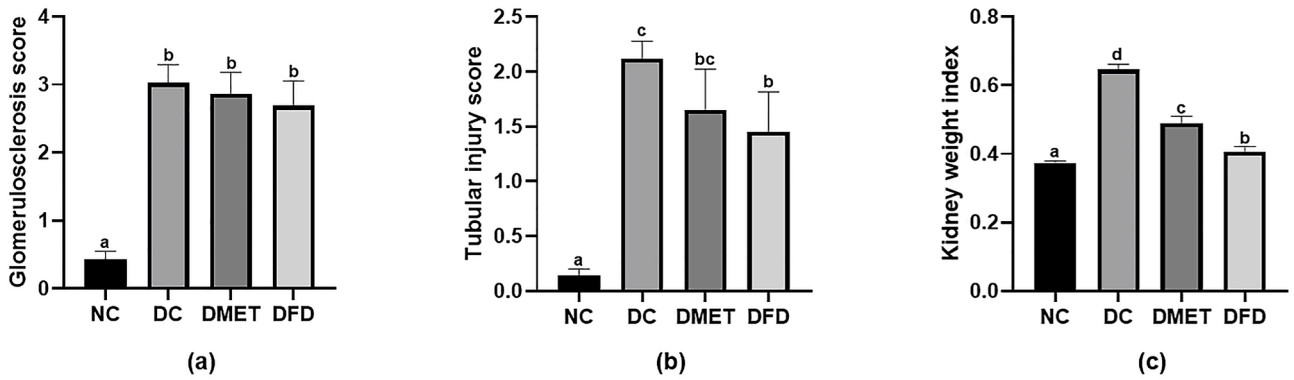

Fig. 5. Kidney histomorphometric. (a) Glomerulosclerosis score, (b) tubular injury score, and (c) kidney weight index. Data are represented as mean ± SD (n = 6). Bars with different superscripts indicate a significant difference ($p < 0.05$).

caspase 8 and MDA levels in the kidneys of diabetic animals that had survived with compromised kidney function and morphological irregularity. Increased serum creatinine levels as well as decreased GFR, urinary creatinine total bilirubin, and GPx further strengthen the association between the IR peak intensity and the existence of kidney failure in STZ-induced diabetic rats.

The second derivative FTIR spectra of the DC animals displayed an intense sharp signal at 1545 cm^{-1} and 1511 cm^{-1}. A significant intensity difference between treatment groups was also observed at these peaks, which correspond to amide II functional groups. These findings were consistent with a study showing that the β-sheet content increased in parallel with the glucose concentration levels (Kristoffersen et al., 2019). An increase in the FTIR peak intensity usually indicates an increase in the amount of the functional group (Du et al., 2018). A study done by Ye *et al.* (2016) demonstrated that FTIR measurement variations in the amide II bands are related to protein aggregation. Higher protein aggregation has been described to positively correlate with intracellular β-sheet contents and apoptosis (Bylund et al., 2013), implying that an increase in amide II peak intensity results from an increased sensitivity of kidney cells to apoptosis. However, some works have reported the nephroprotective role of amide in animal models (Gong et al., 2016). It is important to note that apoptosis is not the only form of programmed cell death, but it is required for kidney cell proliferation and tissue regeneration after injury (Kaushal et al., 2020). Previous findings have shown that the bands related to amide II indeed were more intense in the differentiated kidney cells (Mata-Miranda et al., 2017). Therefore, it is conceivable to suggest that the IR peak of amide II could be a potential spectral marker to indicate the kidney apoptosis index.

HCA and PCA analyzes demonstrated that the treatment effects could also be distinguished at 1246 cm^{-1}, which is dominated by the DNA phosphate backbones. As shown in Table 1, the untreated diabetic rats have a significantly higher peak intensity at 1246 cm^{-1} as compared to the NC groups. A similar observation has been described for the pulmonary hypertension rat model (Staniszewska-Slezak et al., 2015). Sofińska *et al.* reported that increasing the intensity of phosphate vibration indicates DNA fragmentation (Sofińska et al., 2020). High kidney DNA fragmentation has indeed been demonstrated in STZ-induced diabetic rats (Pal et al., 2014). Oxidative stress is considered a cause of DNA fragmentation in chronic kidney disease (Gyurászová et al., 2020). An increase in DNA fragmentation usually correlates with apoptotic progress (Ajayi et al., 2020). This is consistent with our current observation that the 1545 cm^{-1} and 1511 cm^{-1} bands are directly proportional to the band at 1246 cm^{-1}. Another study has nevertheless shown that the apoptotic index is inversely proportional to the spectral area 900-1250 cm^{-1} (Gasparri et al., 2003). However, the study is limited to human HL60 leukemic cells. Therefore, measuring the levels of apoptosis-related proteins and lipid peroxidation in the kidney tissues is essential to support the hypothesis that changes in FTIR spectra absorption bands are reliable for indicating biochemical changes in the kidneys of rats.

GFR is a key indicator of kidney function (Schwartz et al., 2009). We showed that the GFR decreased following STZ injection, which is inversely proportional to the peak intensity at 1545 cm^{-1}, 1511 $cm^{-1,}$ and 1246 cm^{-1}. This observation is consistent with previous reports that long-standing hyperglycemia causes GFR decline (Palatini, 2012; Thomson et al., 2012) and an increase in the amide II and DNA-related regions were associated with chronic kidney diseases (Delanghe et al., 2019; Yu et al., 2017). Interestingly, the DFD animals with lower peak intensity at 1545 cm^{-1}, 1511 cm^{-1}, and 1246 cm^{-1} had significant increases in the GFR over the treatment period. This result is of particular importance because an increase in the GFR implies delayed progression of chronic kidney disease (Okada et al., 2012; Satoh et al., 2010) and adds further evidence demonstrating the potential of FTIR spectroscopy to estimate kidney function.

The role of apoptosis in kidney cell injury has been reported in several studies (Wu et al., 2023; Erekat, 2022). To further investigate the association between the IR spectral changes and the degree of kidney injury, the levels of apoptosis-related proteins in kidney tissue were measured by ELISA. As shown in Table 3, higher values of caspase-8 and caspase-9 were observed in the kidney of DC rats. A similar finding was reported by Pal et al., 2014. The kidney caspase-8 and caspase-9 levels were nevertheless decreased in the DFD and DMET rats that had lower peak intensity at 1545 cm^{-1}, 1511 cm^{-1}, and 1246 cm^{-1} compared to the DC group. There is compelling evidence supporting the link between caspase-8 and β-sheet structure in apoptotic cell death (Tsang et al., 2016; Giri et al., 2003). It has been suggested that the cleavage of protein may contribute to the β-sheet structure, which in turn induces apoptotic cell death by targeting mitochondria. In parallel with FTIR spectra and histological findings, we confirm the nephroprotective effects of *F. deltoidea* extract, thus supporting our hypothesis that the peak appeared at 1545 cm^{-1} and 1511 cm^{-1} could be a reliable spectral marker to indicate the degree of kidney injury.

We showed that MDA levels were increased and the activities of GPx decreased in the kidney of DC rats similar to that reported in previous studies (Gomathi et al., 2014). However, the elevation of kidney SOD levels contradicted previous studies. These findings suggest that STZ promotes kidney injury by increasing intracellular hydrogen peroxide. Hydrogen peroxide (H_2O_2) has been reported to potentiate evoked calcium influx in the podocytes, an important role in the development of kidney damage (Ilatovskaya et al., 2018). It has also been demonstrated that H_2O_2 contributes to kidney cellular injury and necrosis by modulating inflammatory mediators (Liu et al., 2014; Lee et al., 2006). Therefore, the balance of SOD and GPx is more important to counteract the increase in oxidative stress induced by STZ than the level of SOD alone (Li et al., 2000). Intriguingly, *F. deltoidea* extract treatment resulted in the elevation of GPx to SOD ratio as well as a significant

reduction in MDA levels. DNA fragmentation has been reported to positively correlate to MDA levels (Atig et al., 2017). These results indeed demonstrated that animals with lower kidney MDA levels displayed a lower peak intensity at 1246 cm^{-1} than the DC group, evidencing the differences in absorbance intensities recorded by FTIR spectroscopy can be used to quantify oxidative DNA damage.

Histological analysis of the kidney demonstrates STZ caused early onset of glomerulosclerosis, severe tubular degeneration, and tubular necrosis at the cortico-medullary zone. These observations were corroborated by the histomorphometry results for glomerulosclerosis and tubular injury scores, as well as the kidney weight index. Glomerulosclerosis is commonly characterized by distortion of capillary architecture, that is, the leading cause of kidney failure (Chugh et al., 2014). Although capillary loops remain poorly defined in all treated groups, the degree of necrosis of the tubular epithelium was significantly reduced by *F. deltoidea* extract treatment for 77.20 % as compared to the DC group. These histological features were consistent with the findings of FTIR results shown in Fig. 2 and Table 1. Notably, the DFD group that had shown marked improvement in kidney morphology is associated with a significant increase in urinary creatinine, serum total bilirubin, and a decrease in peak intensity at 1545 cm^{-1}, 1511 cm^{-1}, and 1246 cm^{-1}. The serum creatinine decreased to a near-average level. It is worth mentioning that an increase in serum bilirubin levels and decreased serum creatinine usually indicate a nephroprotective effect (Kaur et al., 2016; Mirmohammadlu et al., 2015; Si et al., 2014). Meanwhile, the elevation of bilirubin protects the kidney from systemic oxidative stress in the vascular compartment (Tsai and Tarng, 2018). Taken together, it is reasonable to suggest that *F. deltoidea* extract possesses nephroprotective activity in STZ-induced diabetic rats better than those reported in the metformin-treated rats and FTIR may allow for the detection of treatment effect on the kidney earlier than is morphologically evident.

Conclusion

Treatment with *F. deltoidea* extract ameliorates kidney injury in STZ-treated rats, at least in part, by ameliorating hyperglycemia-mediated oxidative stress and apoptosis. We suggest that the application of FTIR combined with chemometrics can be used to identify biochemical and pathological changes in the kidneys of diabetic rats. We provide evidence that there is a good agreement between the intensity of IR peaks at 1545 cm^{-1}, 1511 cm^{-1}, and 1246 cm^{-1} and kidney function, supporting the use of FTIR in accessing the nephroprotective effect of *F. deltoidea* extract. Further clinical studies are warranted to validate the use of FTIR as an ancillary tool for the diagnosis of kidney disease.

Funding

This work was financially supported by a grant from the Ministry of Higher Education [MOE FRGS: 600-RMI/FRGS 5/3 (325/2019)] and Bio Fluid Sdn Bhd [MIH-(011/2020) 100-TNCPI/PRI 16/6/2 (028/2020)], Faculty of Applied Sciences, Universiti Teknologi MARA, Malaysia.

Data availability

The datasets used and/or analyzed during the current study are available from the corresponding author on reasonable request.

CRediT authorship contribution statement

Nurdiana Samsulrizal: Writing – original draft, Funding acquisition, Data curation. **Noor Syaffinaz Noor Mohamad Zin:** Investigation, Formal analysis. **Nur Syimal`ain Azmi:** Methodology, Investigation. **Mohd Daud Bakar:** Visualization. **Hafandi Ahmad:** Writing – review & editing, Supervision. **Yong-Meng Goh:** Writing – review & editing, Supervision, Conceptualization.

Declaration of competing interest

The authors declare that they have no known competing financial interests or personal relationships that could have appeared to influence the work reported in this paper.

Acknowledgments

We thank Laboratory Animal Facility and Management (LAFAM), Universiti Teknologi MARA for the postoperative care of the animals.

References

Abrahim, N.N., Abdul-Rahman, P.S., Aminudin, N., 2018. The antioxidant activities, cytotoxic properties, and identification of water-soluble compounds of *Ficus deltoidea* leaves. PeerJ. 6, 5694. https://doi.org/10.7717/peerj.5694.

Ajayi, A.F., Akhigbe, R.E., 2020. Codeine-induced sperm DNA damage is mediated predominantly by oxidative stress rather than apoptosis. Redox. Rep. 25 (1), 33–40. https://doi.org/10.1080/13510002.2020.1752003.

Alaofi, A.L., 2020. Sinapic acid ameliorates the progression of streptozotocin (STZ)-induced diabetic nephropathy in rats via NRF2/HO-1 mediated pathways. Front. Pharmacol. 11, 1119, 0.3389/fphar.2020.01119.

Anvarifard, P., Ostadrahimi, A., Ardalan, M., Anbari, M., Ghoreishi, Z., 2023. The effects of propolis on pro-oxidant-antioxidant balance, glycemic control, and quality of life in chronic kidney disease: a randomized, double-blind, placebo-controlled trial. Sci. Rep. 13 (1), 9884. https://doi.org/10.1038/s41598-023-37033-z.

Apriasari, M.L., Nadia, H., Hanifa, N., Utami, J.P., Firdaus, I.W.A.K., 2024. *In vitro* and *in vivo* nephrotoxicity evaluation of the methanol extract of *Ficus deltoidea* Jack Leaf. Trop. J. Nat. Prod. Res. 8 (6), 7514–7519. https://doi.org/10.26538/tjnpr/v8i6.28.

Ashraf, K., Halim, H., Lim, S.M., Ramasamy, K., Sultan, S., 2020. *In vitro* antioxidant, antimicrobial and antiproliferative studies of four different extracts of *Orthosiphon stamineus, Gynura procumbens* and *Ficus deltoidea*. Saudi. J. Biol. Sci. 1, 417–432. https://doi.org/10.1016/j.sjbs.2019.11.003.

Ashtarinezhad, A., Panahyab, A., Mohamadzadehasl, B., Vatanpour, H., Shirazi, F.H., 2015. FT-IR microspectroscopy reveals chemical changes in mice fetus following phenobarbital administration. Iran. J. Pharm. Res. 14, 121–130. https://doi.org/10.22037/ijpr.2015.1721.

Atig, F., Kerkeni, A., Saad, A., Ajina, M., 2017. Effects of reduced seminal enzymatic antioxidants on sperm DNA fragmentation and semen quality of Tunisian infertile men. J. Assist. Reprod. Genet. 34 (3), 373–381. https://doi.org/10.1007/s10815-013-9936-x.

Balan, V., Mihai, C.T., Cojocaru, F.D., Uritu, C.M., Dodi, G., Botezat, D., Gardikiotis, I., 2019. Vibrational spectroscopy fingerprinting in medicine: from molecular to clinical practice. Materials. (Basel) 12 (18), 2884. https://doi.org/10.3390/ma12182884.

Barbieri, M., Chiodini, P., Di Gennaro, P., Hafez, G., Liabeuf, S., Malyszko, J., Mani, L.Y., Mattace-Raso, F., Pepin, M., Perico, N., Simeoni, M., Zoccali, C., Tortorella, G., Capuano, A., Remuzzi, G., Capasso, G., Paolisso, G., 2024. Efficacy of erythropoietin as a neuroprotective agent in CKD-associated cognitive dysfunction: a literature systematic review. Pharmacol. Res. 203, 107146. https://doi.org/10.1016/j.phrs.2024.107146.

Banki, E., Kovacs, K., Nagy, D., Juhasz, T., Degrell, P., Csanaky, K., Kiss, P., Jancso, G., Toth, G., Tamas, A., Reglodi, D., 2014. Molecular mechanisms underlying the Nephroprotective effects of PACAP in diabetes. J. Mol. Neurosci. 54 (3), 300–309. https://doi.org/10.1007/s12031-014-0249-z.

Barraza-Garza, G., Castillo-Michel, H., de la Rosa, L.A., Martinez-Martinez, A., Perez-Leon, J.A., Alvarez-Parrilla, E., 2016. Infrared spectroscopy as a tool to study the antioxidant activity of polyphenolic compounds in isolated rat enterocytes. Oxid. Med. Cell Longev. 9245150. https://doi.org/10.1155/2016/9245150.

Bernardes-Oliveira, E., de Freitas, de Morais, Cornetta, M.D.C.M., Camargo, J.D.A.S., de Lima, Crispim, J.C.O., 2020. Spectrochemical differentiation in gestational diabetes mellitus based on attenuated total reflection Fourier-transform infrared (ATR-FTIR) spectroscopy and multivariate analysis. Sci. Rep. 10 (1), 19259. https://doi.org/10.1038/s41598-020-75539-y.

Borza, D.B., 2017. Glomerular basement membrane heparan sulfate in health and disease: a regulator of local complement activation. Matrix. Biol. 57-58, 299–310. https://doi.org/10.1016/j.matbio.2016.09.002.

Bunawan, H., Amin, N.M., Bunawan, S.N., Baharum, S.N., Mohd Noor, N., 2014. *Ficus deltoidea* Jack: a review on its phytochemical and pharmacological importance. Evid. Based. Complement. Alternat. Med., 902734 https://doi.org/10.1155/2014/902734.

Bylund, J., Annas, A., Hellgren, D., Bjurström, S., Andersson, H., Svanhagen, A., 2013. Amide hydrolysis of a novel chemical series of microsomal prostaglandin E synthase-1 inhibitors induces kidney toxicity in the rat. Drug Metab. Dispos. 41 (3), 634–641. https://doi.org/10.1124/dmd.112.048983.

Chugh, S.S., Macé, C., Clement, L.C., Avila, M.D.N., Marshall, C.B., 2014. Angiopoietin-like 4 based therapeutics for proteinuria and kidney disease. Front. Pharmacol. 5, 23. https://doi.org/10.3389/fphar.2014.00023.

de Oliveira, A., de Oliveira, T., Bobadilla, L., Garcia, C.C.M., Berra, C.M., de Souza-Pinto, N.C., Medeiros, M.H.G., Mascio, P.D., Zatz, R., Loureiro, A.P.M, 2017. Sustained kidney biochemical derangement in treated experimental diabetes: a clue to metabolic memory. Sci. Rep. 7, 40544. https://doi.org/10.1038/srep40544.

Deeds, M.C., Anderson, J.M., Armstrong, A.S., Gastineau, D.A., Hiddinga, H.J., Jahangir, A., Eberhardt, N.L., Kudva, Y.C., 2011. Single dose streptozotocin-induced diabetes: considerations for study design in islet transplantation models. Lab. Anim. 45 (3), 131–140. https://doi.org/10.1258/la.2010.010090.

Delanghe, S.E., De Bruyne, S., De Baene, L., Van Biesen, W., Speeckaert, M.M., Delanghe, J.R., 2019. Estimating the level of carbamoylated plasma non-high-density lipoproteins using infrared spectroscopy. J. Clin. Med. 8 (6), 774. https://doi.org/10.3390/jcm8060774.

Demir, P., Onde, S., Severcan, F., 2015. Phylogeny of cultivated and wild wheat species using ATR-FTIR spectroscopy. Spectrochim. Acta A. Mol. Biomol. Spectrosc. 135C, 757–763. https://doi.org/10.1016/j.saa.2014.07.025.

Dong, Y., Jing, T., Meng, Q., Liu, C., Hu, S., Ma, Y., Liu, Y., Lu, J., Cheng, Y., Wang, D., Teng, L., 2014. Studies on the antidiabetic activities of *Cordyceps militaris* extract in diet-streptozotocin-induced diabetic Sprague-Dawley rats. Biomed. Res. Int., 160980 https://doi.org/10.1155/2014/160980, 2014.

Drozdz, A., Matusiak, K., Setkowicz, Z., Ciarach, M., Janeczko, K., Sandt, C., Borondics, F., Horak, D., Babic, M., Chwiej, J., 2020. FTIR microspectroscopy revealed biochemical changes in liver and kidneys as a result of exposure to low dose of iron oxide nanoparticles. Spectrochim. Acta a Mol. Biomol. Spectrosc. 236, 118355. https://doi.org/10.1016/j.saa.2020.118355.

Du, X.J., Sun, Y.Y., Pan, D.D., Wang, Y., Ou, C.R., Cao, J.X., 2018. The effect of structural change on the digestibility of sarcoplasmic proteins in Nanjing dry-cured duck during processing. Poult. Sci. 97 (12), 4450–4457. https://doi.org/10.3382/ps/pey316.

Elsacker, E., Vandelook, S., Brancart, J., Peeters, E., De Laet, L, 2019. Mechanical, physical and chemical characterisation & of mycelium-based composites with different types of lignocellulosic substrates. PLoS. One 14 (7), 0213954. https://doi.org/10.1371/journal.pone.0213954.

Erekat, N.S., 2022. Programmed cell death in diabetic nephropathy: a review of apoptosis, autophagy, and necroptosis. Med. Sci. Monit. 28, e937766. https://doi.org/10.12659/MSM.937766.

Farsi, E., Ahmad, M., Hor, S.Y., Ahamed, M.B., Yam, M.F., Asmawi, M.Z., Khoo, B.Y., 2014. Standardized extract of *Ficus deltoidea* stimulates insulin secretion and blocks hepatic glucose production by regulating the expression of glucose-metabolic genes in streptozotocin-induced diabetic rats. BMC. Complement. Altern. Med. https://doi.org/10.1186/1472-6882-14-220, 2014.

Farsi, E., Shafaei, A., Hor, S.Y., Ahamed, M.B., Yam, M.F., Asmawi, M.Z., Ismail, Z., 2013. Genotoxicity and acute and subchronic toxicity studies of a standardized methanolic extract of *Ficus deltoidea* leaves. Clinics. (Sao Paulo) 68 (6), 865–875. https://doi.org/10.6061/clinics/2013(06)23.

Gasparri, F., Muzio, M., 2003. Monitoring of apoptosis of HL60 cells by Fourier-transform infrared spectroscopy. Biochem. J. 369 (Pt 2), 239–248. https://doi.org/10.1042/BJ20021021.

Giri, K., Ghosh, U., Bhattacharyya, N.P., Basaka, S., 2003. Caspase 8 mediated apoptotic cell death induced by β-sheet forming polyalanine peptides. FEBS Lett. 555 (2), 380–384. https://doi.org/10.1016/s0014-5793(03)01294-8.

Gomathi, D., Kalaiselvi, M., Ravikumar, G., Devaki, K., Uma, C., 2014. Evaluation of antioxidants in the kidney of streptozotocin induced diabetic rats. Indian J. Clin. Biochem. 29 (2), 221–226. https://doi.org/10.1007/s12291-013-0344-x.

Gong, X., Duan, Y., Zheng, J., Wang, Y., Wang, G., Norgren, S., Hei, T.K., 2016. Nephroprotective effects of N-acetylcysteine amide against contrast-induced nephropathy through upregulating Thioredoxin-1, inhibiting ASK1/p38MAPK pathway, and suppressing oxidative stress and apoptosis in rats. Oxid. Med. Cell Longev. 2016, 8715185. https://doi.org/10.1155/2016/8715185.

González-Pérez, A., Saez, M., Vizcaya, D., Lind, M., Garcia Rodriguez, L., 2021. Incidence and risk factors for mortality and end-stage renal disease in people with type 2 diabetes and diabetic kidney disease: a population-based cohort study in the UK. BMJ Open. Diabetes. Res. Care 9 (1), e002146. https://doi.org/10.1136/bmjdrc-2021-002146.

Guo, J., Zheng, H.J., Zhang, W., Lou, W., Xia, C., Han, X.T., Huang, W.J., Zhang, F., Wang, Y., Liu, W.J., 2020. Accelerated kidney aging in diabetes mellitus. Oxid. Med. Cell. Longev. 2020, 1234059. https://doi.org/10.1155/2020/1234059.

Gyurászová, M., Gurecká, R., Bábíčková, J., Tóthová, Ľ., 2020. Oxidative stress in the pathophysiology of kidney disease: Implications for noninvasive monitoring and identification of biomarkers. Oxid. Med. Cell Longev., 5478708 https://doi.org/10.1155/2020/5478708.

Hirata, Y., Yamamoto, E., Tokitsu, T., Fujisue, K., Kurokawa, H., Sugamura, K., Sakamoto, K., Tsujita, K., Tanaka, T., Kaikita, K., Hokimoto, S., Sugiyama, S., Ogawa, H., 2015. The pivotal role of a novel biomarker of reactive oxygen species in chronic kidney disease. Medicine (Baltimore) 94 (25), e1040. https://doi.org/10.1097/MD.0000000000001040.

Holman, H.Y.N., Martin, M.C., McKinney, W.R., 2003. Tracking chemical changes in a live cell: biomedical applications of SR-FTIR spectromicroscopy. Spectrosc. 17, 486940. https://doi.org/10.1155/2003/486940.

Ilatovskaya, D.V., Blass, G., Palygin, O., Levchenko, V., Pavlov, T.S., Grzybowski, M.N., Winsor, K., Shuyskiy, L.S., Geurts, A.M., Cowley, A.W., Birnbaumer, L., Staruschenko, A., 2018. A NOX4/TRPC6 pathway in podocyte calcium regulation and renal damage in diabetic kidney disease. J. Am. Soc. Nephrol. 29 (7), 1917–1927. https://doi.org/10.1681/ASN.2018030280.

Jain, P.G., Nayse, P.G., Patil, D.J., Shinde, S.D., Surana, S.J., 2020. The possible antioxidant capabilities of formononetin in guarding against streptozotocin-induced diabetic nephropathy in rats. Futur. J. Pharm. Sci. 6, 53. https://doi.org/10.1186/s43094-020-00071-9.

Jensen, T.L., Kiersgaard, M.K., Sørensen, D.B., Mikkelsen, L.F., 2013. Fasting of mice: a review. Lab. Anim. 47 (4), 225–240. https://doi.org/10.1177/0023677213501659.

Jiménez-Osorio, A.S., García-Niño, W.R., González-Reyes, S., Álvarez-Mejía, A.E., Guerra-León, S., Salazar-Segovia, J., Falcón, I., Montes de Oca-Solano, H., Madero, M., Pedraza-Chaverri, J., 2016. The effect of dietary supplementation with curcumin on redox status and nrf2 activation in patients with nondiabetic or diabetic proteinuric chronic kidney disease: a pilot study. J. Ren. Nutr. 26 (4), 237–244. https://doi.org/10.1053/j.jrn.2016.01.013.

Kaur, R., Sodhi, R.K., Aggarwal, N., Kaur, J., Jain, U.K., 2016. Renoprotective effect of lansoprazole in streptozotocin-induced diabetic nephropathy in Wistar rats. Naunyn-Schmiedeberg's Arch. Pharmacol. 389 (1), 73–85. https://doi.org/10.1007/s00210-015-1182-6.

Kaushal, G.P., Chandrashekar, K., Juncos, L.A., Shah, S.V., 2020. Autophagy function and regulation in kidney disease. Biomolecules. 10 (1), 100. https://doi.org/10.3390/biom10010100.

Kristoffersen, K.A., Liland, K.H., Böcker, U.S., Wubshet, G., Lindberg, D., Horn, S.J., Afseth, N.K., 2019. FTIR-based hierarchical modeling for prediction of average molecular weights of protein hydrolysates. Talanta 205, 120084. https://doi.org/10.1016/j.talanta.2019.06.084.

Lee, H.T., Kim, M., Jan, M., Emala, C.W., 2006. Anti-inflammatory and antinecrotic effects of the volatile anesthetic sevoflurane in kidney proximal tubule cells. Am. J. Physiol. Renal. Physiol. 291 (1), F67–F78. https://doi.org/10.1152/ajprenal.00412.2005.

Li, S., Yan, T., Yang, J.Q., Oberley, T.D., Oberley, L.W., 2000. The role of cellular glutathione peroxidase redox regulation in the suppression of tumor cell growth by manganese superoxide dismutase. Cancer Res. 60 (14), 3927–3939.

Liu, D., Huang, P., Li, X., Ge, M., Luo, G., Hei, Z., 2014. Using inflammatory and oxidative biomarkers in urine to predict early acute kidney injury in patients undergoing liver transplantation. Biomarkers 19 (5), 424–429. https://doi.org/10.3109/1354750X.2014.924997.

Lowry, O.H., Rosebrough, N.J., Farr, A.L., Randall, R.J., 1951. Protein measurement with the Folin phenol reagent. J. Biol. Chem. 193 (1), 265–275.

Lubczak, R., 2008. Bifunctional oligoetherols with carbazole ring. J. Appl. Polym. Sci. 110(6), 3501-3507. https://doi.org/10.1002/app.28935.

Mata-Miranda, M.M., Guerrero-Ruiz, M., Gonzalez-Fuentes, J.R., Hernandez-Toscano, C. M., Garcia-Andino, J.R., Sanchez-Brito, M., Vazquez-Zapien, G.J., 2019. Characterization of the biological fingerprint and identification of associated parameters in stress fractures by FTIR spectroscopy. Biomed. Res. Int., 1241452 https://doi.org/10.1155/2019/1241452, 2019.

Mata-Miranda, M.M., Vazquez-Zapien, G.J., Rojas-Lopez, M., Sanchez-Monroy, V., Perez-Ishiwara, D.G., Delgado-Macuil, R.J., 2017. Morphological, molecular and FTIR spectroscopic analysis during the differentiation of kidney cells from pluripotent stem cells. Biol. Res. 50, 14. https://doi.org/10.1186/s40659-017-0119-6.

Mihoubi, W., Sahli, E., Gargouri, A., Amiel, C., 2017. FTIR spectroscopy of whole cells for the monitoring of yeast apoptosis mediated by p53 over-expression and its suppression by *Nigella sativa* extracts. PLoS. One. 12 (7), 0180680. https://doi.org/10.1371/journal.pone.0180680.

Mirmohammadlu, M., Hosseini, S., Kamalinejad, M., Esmaeili Gavgani, M., Noubarani, M., Eskandari, M.R., 2015. Hypolipidemic, hepatoprotective and renoprotective effects of *Cydonia oblonga* mill. fruit in streptozotocin-induced diabetic rats. Iran. J. Pharm. Res. 14 (4), 1207–1214. https://doi.org/10.22037/IJPR.2015.1747.

ur Movasaghi, Z., Rehman, S., Rehman, I., 2008. Fourier transform infrared (FT-IR) spectroscopy of biological tissues. Appl. Spectrosc. Rev. 43, 134–179. https://doi.org/10.1080/05704920701829043.

Noshahr, Z.S., Salmani, H., Khajavi Rad, A., Sahebkar, A., 2020. Animal models of diabetes-associated renal injury. J. Diabetes. Res., 9416419 https://doi.org/10.1155/2020/9416419, 2020.

Nugroho, R.A., Aryani, R., Manurung, H., Rudianto, R., Prahastika, W., Juwita, A., Alfarisi, A.K., Pusparini, N.A.O., Lalong, A., 2020. Acute and subchronic toxicity study of the ethanol extracts from *Ficus deltoidea* leaves in male mice. Open. Access. Maced. J. Med. Sci. 8, 76–83. https://doi.org/10.3889/oamjms.2020.3989.

Nurdiana, S., Goh, Y.M., Ahmad, H., Dom, S.M., Syimal'ain Azmi, N., Noor Mohamad Zin, N.S., Ebrahimi, M., 2017. Changes in pancreatic histology, insulin secretion and oxidative status in diabetic rats following treatment with *Ficus deltoidea* and vitexin. BMC. Complement. Altern. Med. 17 (1), 290. https://doi.org/10.1186/s12906-017-1762-8.

Nurdiana, S., Goh, Y.M., Hafandi, A., Dom, S.M., Nur Syimal'ain, A., Noor Syaffinaz, N. M., Ebrahimi, M., 2017. Improvement of spatial learning and memory, cortical gyrification patterns and brain oxidative stress markers in diabetic rats treated with *Ficus deltoidea* leaf extract and vitexin. J. Tradit. Complement. Med. 8 (1), 190–202. https://doi.org/10.1016/j.jtcme.2017.05.006.

Okada, R., Yasuda, Y., Tsushita, K., Wakai, K., Hamajima, N., Matsuo, S., 2012. Glomerular hyperfiltration in prediabetes and prehypertension. Nephrol. Dial. TransPlant 27 (5), 1821–1825. https://doi.org/10.1093/ndt/gfr651.

Pal, P.B., Sinha, K., Sil, P.C., 2014. Mangiferin attenuates diabetic nephropathy by inhibiting oxidative stress mediated signaling cascade, TNFα related and mitochondrial dependent apoptotic pathways in streptozotocin-induced diabetic rats. PLoS. One 9 (9), 107220. https://doi.org/10.1371/journal.pone.0107220.

Palatini, P., 2012. Glomerular hyperfiltration: a marker of early renal damage in pre-diabetes and pre-hypertension. Nephrol. Dial. TransPlant 27 (5), 1708–1714. https://doi.org/10.1093/ndt/gfs037.

Petibois, C., Rigalleau, V., Melin, A.M., Perromat, A., Cazorla, G., Gin, H., Déléris, G., 1999. Determination of glucose in dried serum samples by Fourier-transform infrared spectroscopy. Clin. Chem. 45 (9), 1530–1535. https://doi.org/10.1093/clinchem/45.9.1530.

Pezzaniti, J.L., Jeng, T.W., McDowell, L., Oosta, G.M., 2001. Preliminary investigation of near-infrared spectroscopic measurements of urea, creatinine, glucose, protein, and

ketone in urine. Clin. Biochem. 34 (3), 239–246. https://doi.org/10.1016/s0009-9120(01)00198-9.
Pillai, A., Fulmali, D., 2023. A narrative review of new treatment options for diabetic nephropathy. Cureus. 15 (1), e33235. https://doi.org/10.7759/cureus.33235.
Sablinskas, V., Bandzeviciute, R., Velicka, M., Ceponkus, J., Urboniene, V., Jankevicius, F., Laurinavičius, A., Dasevičius, D., Steiner, G., 2020. Fiber attenuated total reflection infrared spectroscopy of kidney tissue during live surgery. J. Biophotonics. 13 (7), e202000018. https://doi.org/10.1002/jbio.202000018.
Salleh, N., Ahmad, V.N., 2013. *In-vitro* effect of *Ficus deltoidea* on the contraction of isolated rat's uteri is mediated via multiple receptors binding and is dependent on extracellular calcium. BMC. Complement. Altern. Med. 13, 359. https://doi.org/10.1186/1472-6882-13-359.
Samouillan, V., Revuelta-López, E., Soler-Botija, C., Dandurand, J., Benitez-Amaro, A., Nasarre, L., de Gonzalo-Calvo, D., Bayes-Genis, A., Lacabanne, C., Llorente-Cortés, V., 2017. Conformational and thermal characterization of left ventricle remodeling post-myocardial infarction. Biochim. Biophys. Acta Mol. Basis. Dis. 1863 (6), 1500–1509. https://doi.org/10.1016/j.bbadis.2017.02.025.
Sari, D.C.R., Putri, M.W., Leksono, T.P., Chairunnisa, N., Reynaldi, G.N., Simanjuntak, B. C., Debora, J., Yunus, J., Arfian, N., 2020. Calcitriol ameliorates kidney injury through reducing podocytopathy, tubular injury, inflammation and fibrosis in 5/6 subtotal nephrectomy model in rats. Kobe J. Med. Sci. 65 (5), E153–E163.
Satoh, M., Kobayashi, S., Kuwabara, A., Tomita, N., Sasaki, T., Kashihara, N., 2010. *In vivo* visualization of glomerular microcirculation and hyperfiltration in streptozotocin-induced diabetic rats. Microcirculation. 17 (2), 103–112. https://doi.org/10.1111/j.1549-8719.2009.00010.x.
Schwartz, G.J., Muñoz, A., Schneider, M.F., Mak, R.H., Kaskel, F., Warady, B.A., Furth, S. L., 2009. New equations to estimate GFR in children with CKD. J. Am. Soc. Nephrol. 20 (3), 629–637. https://doi.org/10.1681/ASN.2008030287.
Shen, Y.C., Davies, A.G., Linfield, E.H., Taday, P.F., Arnone, D.D., Elsey, T.S., 2003. Determination of glucose concentration in whole blood using Fourier-transform infrared spectroscopy. J. Biol. Phys. 29 (2-3), 129–133. https://doi.org/10.1023/A:1024480423056.
Shepard, B.D., 2019. Sex differences in diabetes and kidney disease: mechanisms and consequences. Am. J. Physiol. Renal. Physiol. 317 (2), F456–F462. https://doi.org/10.1152/ajprenal.00249.2019.
Si, X., Li, P., Zhang, Y., Zhang, Y., Lv, W., Qi, D., 2014. Renoprotective effects of *Olmesartan medoxomil* on diabetic nephropathy in streptozotocin-induced diabetes in rats. Biomed. Rep. 2 (1), 24–28. https://doi.org/10.3892/br.2013.183.
Singh, A., Ramnath, R.D., Foster, R.R., Wylie, E.C., Fridén, V., Dasgupta, I., Haraldsson, B., Welsh, G.I., Mathieson, P.W., Satchell, S.C., 2013. Reactive oxygen species modulate the barrier function of the human glomerular endothelial glycocalyx. PLoS. One 8 (2), e55852. https://doi.org/10.1371/journal.pone.0055852.
Sofińska, K., Wilkosz, N., Szymoński, M., Lipiec, E., 2020. Molecular spectroscopic markers of DNA damage. Molecules. 25 (3), 561. https://doi.org/10.3390/molecules25030561.
Song, C.L., Vardaki, M.Z., Goldin, R.D., Kazarian, S.G., 2019. Fourier transform infrared spectroscopic imaging of colon tissues: evaluating the significance of amide I and C-H stretching bands in diagnostic applications with machine learning. Anal. Bioanal. Chem. 411 (26), 6969–6981. https://doi.org/10.1007/s00216-019-02069-6.
Staniszewska-Slezak, E., Fedorowicz, A., Kramkowski, K., Leszczynska, A., Chlopicki, S., Baranska, M., Malek, K., 2015. Plasma biomarkers of pulmonary hypertension identified by Fourier transform infrared spectroscopy and principal component analysis. Analyst 140, 2273–2279. https://doi.org/10.1039/c4an01864h.
Sulaiman, M.R., Hussain, M.K., Zakaria, Z.A., Somchit, M.N., Moin, S., Mohamad, A.S., Israf, D.A., 2008. Evaluation of the antinociceptive activity of *Ficus deltoidea* aqueous extract. Fitoterapia 79 (7-8), 557–561. https://doi.org/10.1016/j.fitote.2008.06.005.
Tahara, A., Matsuyama-Yokono, A., Nakano, R., Someya, Y., Shibasaki, M., 2008. Hypoglycaemic effects of antidiabetic drugs in streptozotocin-nicotinamide-induced mildly diabetic and streptozotocin-induced severely diabetic rats. Basic Clin. Pharmacol. Toxicol. 103 (6), 560–568. https://doi.org/10.1111/j.1742-7843.2008.00321.x.
Takemori, H., Hamamoto, A., Isogawa, K., Ito, M., Takagi, M., Morino, H., Miura, T., Oshida, K., Shibata, T., 2020. Mouse model of metformin-induced diarrhea. BMJ Open Diab. Res. Ca. 8 (1), 000898. https://doi.org/10.1136/bmjdrc-2019-000898.
Thomson, S.C., Rieg, T., Miracle, C., Mansoury, H., Whaley, J., Vallon, V., Singh, P., 2012. Acute and chronic effects of SGLT2 blockade on glomerular and tubular function in the early diabetic rat. Am. J. Physiol. Regul. Integr. Comp. Physiol. 302 (1), R75–R83. https://doi.org/10.1152/ajpregu.00357.2011.
Tsai, M.T., Tarng, D.C., 2018. Beyond a measure of liver function-bilirubin acts as a potential cardiovascular protector in chronic kidney disease patients. Int. J. Mol. Sci. 20 (1), 117. https://doi.org/10.3390/ijms20010117.
Tsang, J.L., Jia, S.H., Parodo, J., Plant, P., Lodyga, M., Charbonney, E., Szaszi, K., Kapus, A., Marshall, J.C., 2016. Tyrosine phosphorylation of caspase-8 abrogates its apoptotic activity and promotes activation of c-Src. PLoS. One 11 (4), e0153946. https://doi.org/10.1371/journal.pone.0153946.
Wang, Y.J., Xie, X.S., Feng, S.G., Long, Q.X., Ai, N., Wang, B.F., 2014. [Causes of Death in STZ-Induced Rat Models of Diabetes Mellitus], 45. Sichuan Da Xue Xue Bao Yi Xue Ban, pp. 691–695.
Wang-Fischer, Y., Garyantes, T., 2018. Improving the reliability and utility of streptozotocin-induced rat diabetic model. J. Diabetes. Res., 8054073 https://doi.org/10.1155/2018/8054073.
Wu, T., Ding, L., Andoh, V., Zhang, J., Chen, L., 2023. The mechanism of hyperglycemia-induced renal cell injury in diabetic nephropathy disease: an update. Life (Basel) 13 (2), 539. https://doi.org/10.3390/life13020539.
Ye, S., Ruan, P., Yong, J., Shen, H., Liao, Z., Dong, X., 2016. The impact of HbA1c level of type 2 diabetics on the structure of haemoglobin. Sci. Rep. 6, 33352. https://doi.org/10.1038/srep33352.
Yu, M., Rich, P., Foreman, L., Smith, J., Yu, M.S., Tanna, A., Dibbur, V., Unwin, R., Tam, F.W.K., 2017. Label free detection of sensitive mid-infrared biomarkers of glomerulonephritis in urine using Fourier transform infrared spectroscopy. Sci. Rep. 7, 4601. https://doi.org/10.1038/s41598-017-04774-7.